PERGAMON

Chaos, Solitons and Fractals 16 (2003) 409–416

CHAOS
SOLITONS & FRACTALS

www.elsevier.com/locate/chaos

Timing noise effects on dynamical localization

Windell H. Oskay [1], Daniel A. Steck [2], Mark G. Raizen *

Department of Physics and Center for Nonlinear Dynamics, The University of Texas at Austin, Austin, TX 78712-1081, USA

Abstract

The quantum kicked rotor is studied experimentally in an atom-optics setting, where we observe the center-of-mass motion of cold cesium atoms. Dynamical localization in this system typically suppresses classical diffusive motion, but is susceptible to the addition of various forms of noise. We study in detail the effects of timing noise, where variations are introduced to the times at which the kicks occur. This noise is particularly interesting because it does not directly induce momentum diffusion. However, it is found that the addition of timing noise efficiently destroys both the classical correlations that give rise to fluctuations in the classical diffusion rate as well as quantum coherences that lead to dynamical localization.

The interface between quantum and classical dynamics serves as a testing ground for decoherence and is a central feature of mesoscopic physics. It is believed that decoherence, the destruction of quantum interferences, is necessary to reconcile the distinctly different behavior in the quantum and classical limits [1]. Experimental progress towards understanding decoherence has been made on a number of different fronts. One system that has the advantage of conceptual simplicity is a perturbed atom interferometer [2,3], where spontaneous scattering introduces dissipation into the system. Decoherence has also been observed with Rydberg atoms coupled to microwave cavities [4] and motional Schrödinger cat states in an ion trap [5].

One of the most interesting settings in which to study correspondence is a classically chaotic system, where quantum effects suppress classical diffusive motion [6]. While the majority of research in decohering effects on "quantum chaos" has been theoretical in nature [7–11], there has been a steadily growing body of experimental work in recent years. Some of the pioneering experiments in this field have been conducted by studying the internal dynamics of Rydberg atoms [12–15]. Mesoscopic condensed-matter systems have provided another important testing ground [16]. Recent great advances in atom optics, the manipulation of atomic de Broglie waves, have also made it possible to study quantum dynamics by observing the center-of-mass motion of cold atoms [17,18]. Here, laboratory tests have allowed the direct observation of such phenomena as dynamical localization [19], quantum resonances [20], and chaos-assisted tunneling [21].

Of particular interest is dynamical localization [22], a quantum suppression of classically chaotic (diffusive) motion. A prototypical system is the kicked rotor, or standard map, which has been a model system for the study of both classical and quantum chaos. The kicked rotor is a particularly suitable system for experimental study because it can be directly realized by exposing cold atoms to a pulsed standing wave of light. Classical particles in such a chaotic potential tend to exhibit diffusive behavior, where the energy of the system grows linearly as a function of time. On the other hand, quantum particles in the same potential exhibit diffusive motion for only a short time, after which the energy

* Corresponding author.
E-mail address: raizen@physics.utexas.edu (M.G. Raizen).
[1] Present address: Time & Frequency Division, Natl. Inst. Standards & Technology, 325 Broadway, Boulder, CO 80305, USA.
[2] Present address: Los Alamos National Laboratory, Theoretical Division (T-8), MS B285, Los Alamos NM 87545, USA.

0960-0779/03/$ - see front matter
PII: S0960-0779(02)00302-8

growth slows down. The contrasting behavior in the quantum and classical limits makes the system attractive for the study of quantum–classical correspondence.

In previous work we observed the effects of two different types of perturbations to the kicked-rotor system, both of which are capable of disturbing the fragile quantum coherences that cause dynamical localization. The first perturbation is a simple form of amplitude noise, which is added to the kicked-rotor experiment by allowing variation in the strength of the individual kicks [23]. In this case, we have observed a transition from quantum to classical behavior as the noise level is increased. For strong enough driving, we observed atomic motion that is consistent with fully classical dynamics over the time scales of our experiments [24,25]. The second type of perturbation is a dissipative interaction that is introduced by allowing the atoms to scatter near-resonant light [23]. The introduction of dissipative forces complicates the dynamics considerably and makes the interpretation of the results more difficult. In our experiments with dissipation, optical molasses light was used to induce spontaneous emission but also led to an overall cooling effect. In similar experiments conducted elsewhere [26], the light used to introduce dissipation may have instead led to an overall heating effect. Additionally, an optical analogy of the kicked-rotor system has been used to study the effects of noise in this system [27]. Outside of the kicked-rotor system, we have studied amplitude noise in a different setting, to observe its effects on chaos-assisted tunneling [28]. In this case, the noise breaks the coherences that lead to quantum tunneling between regions of phase space.

We now observe the effects of an additional variety of noise on the kicked rotor. Instead of changing the amplitude of the individual kicks, we allow variation in the timing of the kicks. In this case, we see a transition from quantum behavior to (qualitatively) classical behavior, as occurs in the case of amplitude noise. The nature of the timing noise sequence and improvements to the experimental apparatus contribute to an increase in the signal-to-noise ratio in this data set, as compared to the earlier results with amplitude noise.

In our experiments, we study the center-of-mass motion of ground-state cesium atoms in a modulated 1D optical lattice. The optical lattice consists of a standing wave of light from a Ti:sapphire laser. With the proper choices of laser intensity and detuning from atomic resonance, the conservative light forces on the atom can be significant while the dissipative interactions can simultaneously be made minor enough to permit a detailed study of coherent quantum dynamics. In the far-detuned limit, the atom remains in the ground state and its behavior is that of a point particle in the external optical potential [17]. The well depth of the optical dipole potential (ac Stark shift) depends upon the intensity of the light, and so the standing wave interference pattern leads to a spatially dependent force upon the atom. We may write the Hamiltonian for an atom with position x and momentum p as

$$H(x,p) = \frac{p^2}{2m} + V_0 \cos(2k_{\mathrm{L}}x), \tag{1}$$

where m is the mass of the atom, V_0 is the well depth of the potential, and k_{L} is the wave number of the light. This Hamiltonian describes dynamics that are equivalent to that of a simple pendulum, where the position and linear momentum of the atom in the optical lattice play the roles of the pendulum angle and angular momentum, respectively.

Our potentials are created dynamically using light gated by an acousto-optic modulator (AOM) so that we have a fine degree of control over the intensity of the light. In the kicked-rotor experiments, we modulate the intensity of the optical lattice as a series of short pulses with period T. In this case we have the kicked-rotor Hamiltonian

$$H(x,p,t) = \frac{p^2}{2m} + V_0 \cos(2k_{\mathrm{L}}x) \sum_n F(t-nT), \tag{2}$$

where $F(t)$ is a pulse shape function of unit amplitude and duration t_{p}, and $t_{\mathrm{p}} \ll T$.

It is straightforward to transform into a set of scaled (natural) units that contain the minimum number of constants and facilitate comparison with theoretical models. Let us define the transformations as $x' = 2k_{\mathrm{L}}x$, $t' = t/T$, $p' = p\bar{k}/2\hbar k_{\mathrm{L}}$, $f(t') = F(t)/\eta$, $K = (\bar{k}/\hbar)\eta T V_0$, and $H' = (\bar{k}/\hbar)TH$. The pulse integral $\eta = \frac{1}{T}\int_{-\infty}^{\infty} F(t)\,\mathrm{d}t$, is taken such that $\eta \propto t_{\mathrm{p}}$ and $\int_{-\infty}^{\infty} f(t)\,\mathrm{d}t = 1$. We have also defined the constant $\bar{k} = 8\omega_{\mathrm{r}}T$, where the recoil frequency $\omega_{\mathrm{r}} = \hbar k_{\mathrm{L}}^2/2m$ contains all of the fixed atomic parameters. If we examine the commutation relation $[x',p'] = (\bar{k}/\hbar)[x,p] = i\bar{k}$, we find that $\bar{k}$ plays the role of a scaled Planck constant that tells us the relative action scale of the system compared to $\hbar$. Under these transformations, we may rewrite the kicked-rotor Hamiltonian as

$$H(x,p,t) = \frac{p^2}{2} + K\cos x \sum_n f(t-n), \tag{3}$$

after dropping the primes. The dynamics of the classical kicked rotor are completely specified by the sole parameter K, the stochasticity parameter. For $K \gtrsim 4$, where most of our experiments take place, the kicked-rotor system is predominantly chaotic. The dynamics of the quantum kicked rotor are governed by both K and $\bar{k}$.

As a minor digression, consider the limit where the pulse function is a δ-function so that $t_p \to 0$ while K is constant. In this limit the Hamiltonian becomes that of the δ-kicked rotor, a paradigm of classical and quantum chaos. By integrating the δ-kicked-rotor equations of motion over one period of the kicking, they reduce to the standard mapping [29],

$$\begin{aligned} p_{n+1} &= p_n + K \sin x_n, \\ x_{n+1} &= x_n + p_{n+1}, \end{aligned} \tag{4}$$

where (x_n, p_n) and (x_{n+1}, p_{n+1}) are the coordinates of a particle before and after the nth kick. There are some subtle differences between the dynamics in the cases with δ-function pulses and finite-duration pulses like those found in experiments. The most important effect is that in the case of finite-duration pulses, the amount of momentum transfer to a particle during a kick (i.e., the value of K) depends upon the particle's momentum prior to the kick [20]. This effect is minor for the parameters of the present experiments [30], but it can become important for precise comparison with theoretical models [25].

Timing noise is introduced to the pulse sequence by allowing variation in the period T between kicks, which has been held constant in previous experiments. Let us now replace the constant T with a step-dependent period $T_n = T + \delta T_n$, where δT_n is a step-dependent perturbation to the period. We consider only a uniform probability distribution $P(\delta T_n) = 1/\delta T_{p-p}$, if $|\delta T_n| \leqslant \frac{1}{2}\delta T_{p-p}$, and zero otherwise. This uniform distribution is similar to the one implemented for the studies of amplitude noise. The peak-to-peak range δT_{p-p} is specified as a percentage of T, so that 100% noise means that a kick may be displaced by any value in the range $\pm T/2$. In the experiment, we would like to avoid approaching 100% noise so that the pulses, which have nonzero duration, do not overlap. This fact provides a natural limit to the amount of noise that can be applied. As it turns out, we did not approach this limit because the kicked-rotor system is extremely sensitive to timing noise, and we did not need to study levels higher than 20%.

This realization of timing noise is a *cumulative* one. The time that each kick occurs is $T + \delta T_n$ after the *previous* kick, rather than simply being δT_n displaced from the time that the kick would occur in the absence of applied noise. This distinction is important because kicks occurring later in the sequence can potentially become far displaced from their original times. By contrast, the experiments with amplitude noise allowed for variation in the amplitude of each kick, where the range of variation was centered about the mean kick amplitude.

In the kicked-rotor experiments with amplitude noise, the perturbations were applied directly to the value of K. For timing noise, the variation in T enters the classical dynamics in a slightly less obvious manner. The standard map changes under the influence of timing noise to be

$$\begin{aligned} p_{n+1} &= p_n + K \sin x_n, \\ x_{n+1} &= x_n + (1 + \epsilon_n) p_{n+1}, \end{aligned} \tag{5}$$

where $\epsilon_n \equiv \delta T_n / T$. From this modified mapping, it is clear that timing noise enters the equations of motion in a different manner than does amplitude noise. One immediate effect of this is that timing noise is inherently nonperturbative, and even a small value of ϵ_n can cause large changes to the system if p is large. Intuitively, the addition of timing noise should have a substantial effect on the corresponding classical dynamics, since structures in the standard map surface of section are only visible through stroboscopic (periodic) sampling.

In Fig. 1, we show some features of the noisy mapping Eq. (5) for different levels of timing noise. The energy after 35 kicks is plotted as a function of K. For the case with zero added noise, there is a clear oscillation in this curve as a result of classical correlations in the system dynamics [31,32]. The short-term diffusion rates oscillate about the quasi-linear (random-phase approximation) diffusion rate, $E/t = K^2/4$. The classical correlations are gradually destroyed as more noise is added, and the behavior of the system tends towards the quasi-linear limit. An important consequence is that the classical diffusion rate can either increase *or* decrease as the noise level is increased, depending upon the value of K. Fig. 1 illustrates an additional feature of timing noise, which is that it does not cause *intrinsic* momentum diffusion. Whereas amplitude noise can itself lead to diffusion, timing noise changes the diffusion rate only through the destruction of correlations.

The effects of timing noise on the kicked-rotor dynamics are qualitatively similar to those of amplitude noise, where the perturbations gradually destroy both classical correlations and quantum interferences in the system. To examine the effects of timing noise on the quantum dynamics of our experiment, we must note that the variable T enters not only into the definition of K, but also into the definition of $\bar{k}$. For this reason, the (constant) average value $\langle T \rangle$ is used to compute the values of K and $\bar{k}$. Relatively weak levels of timing noise are needed to destroy dynamical localization. However, the noise is only weak in the sense that we do not approach the maximum value of noise that could potentially be applied to the system. A direct comparison between the sensitivity to amplitude noise and timing noise is

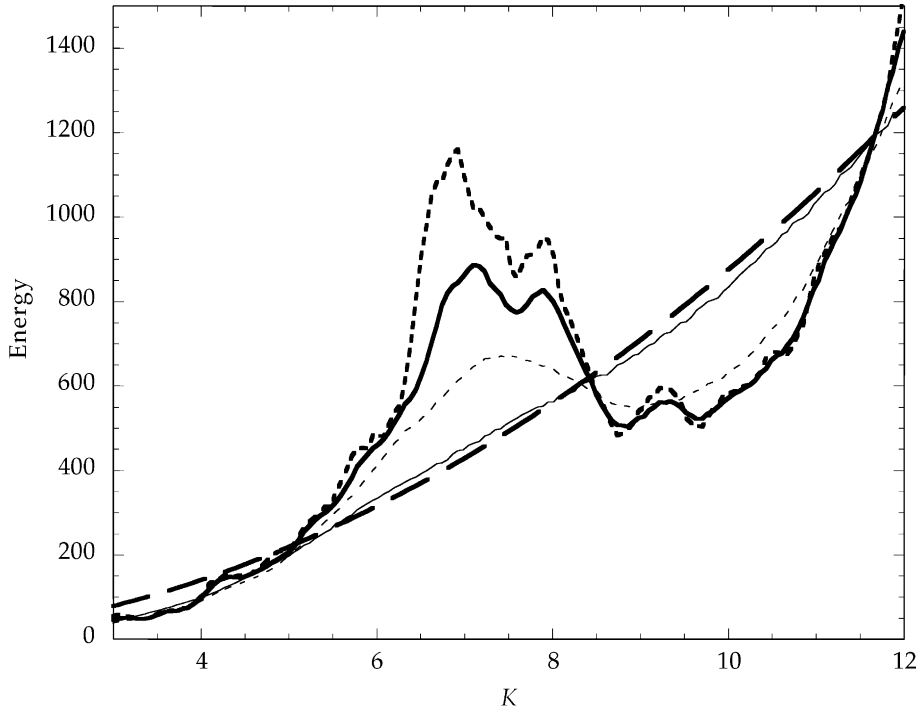

Fig. 1. Timing noise effects on the classical kicked rotor. The modified standard mapping in the presence of timing noise, Eq. (5), is computed for 35 iterations (kicks). The final energy $E = \langle p^2 \rangle / 2$ is plotted as a function of K for various noise levels. The timing noise levels shown are 0% (heavy short dash), 1% (heavy solid), 5% (light dash), and 20% (light solid). For each of the noise cases, the same set of 10^5 initial conditions was used, randomly chosen with x and p within $\pm\pi$. An independent realization of noise was used for each computed trajectory. Also plotted is the quasi-linear diffusion curve, $E = K^2 t/4$ (heavy long dash), where $t = 35$.

complicated by the fact that the timing noise realization is cumulative in nature, whereas the amplitude noise experiments realization was not.

Our experimental apparatus is similar to that described previously [21,25], with several minor modifications. We begin by collecting $\approx 10^6$ cesium atoms from background vapor in a standard magneto-optic trap (MOT) [33], over the course of 4 s. The temperature of atoms released directly from the MOT is of order 10 μK. After collecting the atoms, we turn off the MOT and further cool the atoms with a 3D-lattice cooling scheme similar to that developed by Weiss and his collaborators [34]. The atoms are loaded from the MOT into a 3D, far-detuned, linearly polarized optical lattice. This lattice, tuned 9 GHz to the red of the cesium $6S_{1/2}$, $F = 4 \rightarrow 6P_{3/2}$, $F = 5$ cycling transition, serves to confine the atoms. Once the atoms are confined, the current to the MOT quadrupole magnet coils is turned off. The fields decay with a time scale of several milliseconds, but eddy currents from the shut-off lead to slowly varying fields at the time of the interaction with the 1D standing wave. Although the fields may be on the order of 100 mG, they are not expected to affect the interaction. While in the 3D lattice, the atoms are further cooled in 3D by a weak optical molasses, which is tuned ≈50 MHz to the red of the cycling transition. After the atoms are cooled in this configuration for 5 ms, the far-detuned lattice light is adiabatically extinguished so that the atoms trade their local confinement for a reduction in temperature. After these cooling processes are completed, the atoms are exposed to a brief (150 μs) pulse of "repumping" light tuned directly to the $6S_{1/2}$, $F = 3 \rightarrow 6P_{3/2}$, $F = 4$ resonance to ensure that the atoms are in the $6S_{1/2}$, $F = 4$ state.

The final 1D temperature, as measured along the 1D optical lattice (horizontal) axis, is typically 700 nK, corresponding to a nearly Gaussian momentum distribution with width $\sigma_p = 1.9\hbar k_L$. The temperature of the distribution as measured along the vertical axis is roughly a factor of two higher, due to imbalances in the 3D-lattice beam intensities. We have achieved lower temperatures with 3D-lattice cooling by using a larger detuning and a longer cooling period [21], however increasing the detuning also lowers the well depth V_0.

After cooling and optical pumping, the atoms are exposed to the pulsed standing wave that creates the kicked-rotor potential. The 1D optical lattice light originates from the same laser that generates the 3D lattice, again tuned 9 GHz to the red of resonance. An AOM modulates the continuous-wave laser beam to form the "kicking" pulses. For this set of

experiments, the pulse length was fixed at $t_p = 300$ ns, and the (mean) time between pulses was $T = 20$ μs so that $\bar{k} = 2.08$. The AOM is driven by an arbitrary waveform generator with time resolution of 100 ns, which introduces a fine degree of quantization in the absolute time between any two pulses.

As soon as the kicking sequence is completed, the detection sequence begins. The atoms are allowed to ballistically expand for 15 ms (as measured from the *beginning* of the kick sequence) so that the atomic momentum distribution is converted into a position distribution by the time-of-flight method. The distribution is then frozen into place by an optical molasses and the fluorescence is imaged with a 10 ms exposure on a charge-coupled device camera. The camera image effectively yields the 1D momentum distribution along the standing-wave axis, and we commonly integrate this distribution to find the kinetic energy $E = \langle p^2 \rangle / 2$.

The results of our measurements are shown in Fig. 2. The error bars on the data shown in this paper are purely statistical in nature, representing the standard deviation of the values measured in a series of separate measurements. Each point represents an average over 20 measurements, each with an independent realization of the timing noise. The largest source of uncertainty in our experiment is the absolute value of K, which is only determined to an accuracy of $\pm 10\%$. Also note that for the experimental data reported here, the values of K are scaled by $(2/\bar{k})\sin(\bar{k}/2)$ to simplify comparison with the classical kicked rotor [9,32,35]. There are several sources of systematic errors in the experiment, such as the effects of nonzero pulse duration. These effects are primarily important for comparison with detailed theoretical models, and they are reviewed in detail elsewhere [25].

In Fig. 2 we observe the effects of timing noise on the system energy growth as a function of time, at a constant value of $K = 8$. Without added noise, the energy evolution shows a signature of dynamical localization that appears as a reduction in the rate of energy growth after about 10 kicks. The energy growth does not completely cease, and we

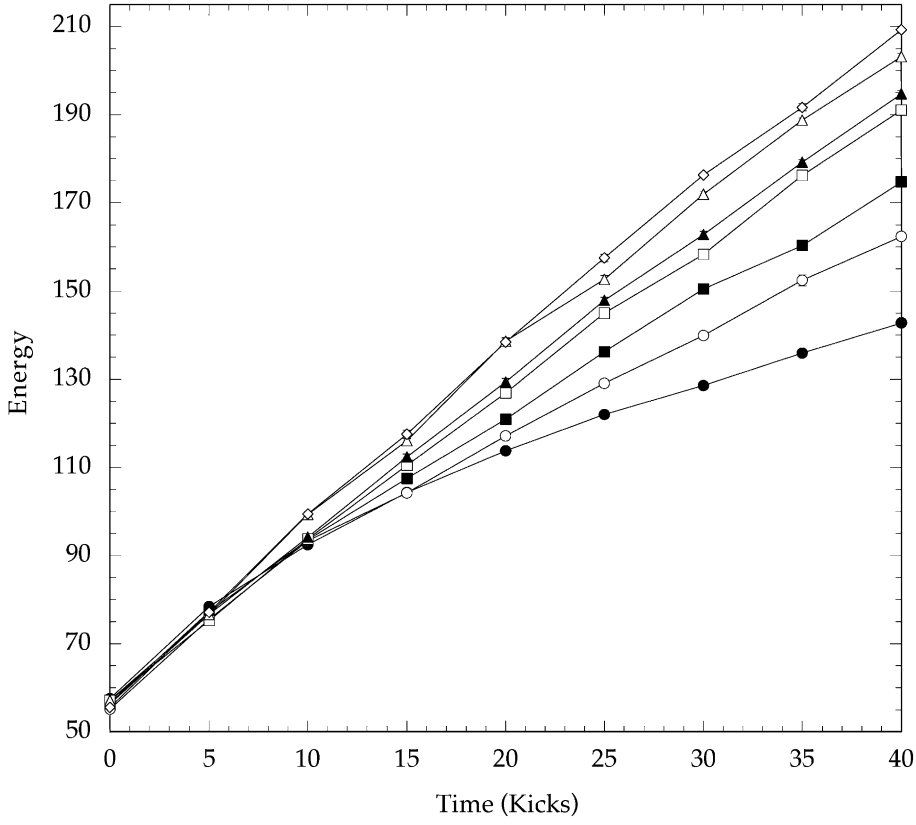

Fig. 2. Timing noise effects on energy evolution in the experiment. The dimensionless energy $E = \langle (p/2\hbar k_L)^2 \rangle / 2$ is plotted as a function of time for several levels of timing noise, near $K = 8$. The noise levels are 0% (filled circles), 0.5% (open circles), 1% (filled squares), 2% (open squares), 3% (filled triangles), 10% (open triangles), and 20% (diamonds), for which the energy values are increasing monotonically at this value of K. The data points are collected for every five kicks, and the lines connect these points to guide the eye. The statistical error bars on most of the data points are too small to be clearly resolved in this plot.

attribute this diffusion to residual decohering processes such as phase noise in the standing wave. For as little as 0.5% added timing noise, there is a significant change in the long-time diffusion rate. The energy growth begins to saturate when we add timing noise at about the 3% level. This is in contrast to the amplitude noise experiments, where we had to make severe changes to the pulse sequence before the energy growth saturated. This saturation phenomenon is to some degree an effect of the particular value of K that we have chosen, in this case near $K = 8$.

We also measured the ensemble energy as a function of K after a constant number of kicks (35 for the data shown here), and the results are shown in Fig. 3. This figure bears some similarities to its classical counterpart, Fig. 1. It is clear that the presence of noise gradually washes out the oscillations in the curves as the noise level increases. The most important difference between the experiment and the classical simulations is that the energy in the experiment grows as low levels of noise are applied, independent of the value of K. We believe that this results from the destruction of dynamical localization, which begins to bring the energy values closer to those that we would expect from classical dynamics. As the level of noise increases, the energy at certain K values does eventually decrease along with the classical model, but does not go below the zero-noise energy level. Quantitative comparison between this figure and Fig. 1 is not trivial because of a number of systematic effects that generally serve to reduce the effective energies that we measure in the experiments [25].

For the value of K chosen in Fig. 2, which is located in the first local minimum of the $E(K)$ curve, most of the energy growth occurs by the 3% noise level. Near the first local maximum of the curve in Fig. 3 (near $K = 2\pi$), the energy

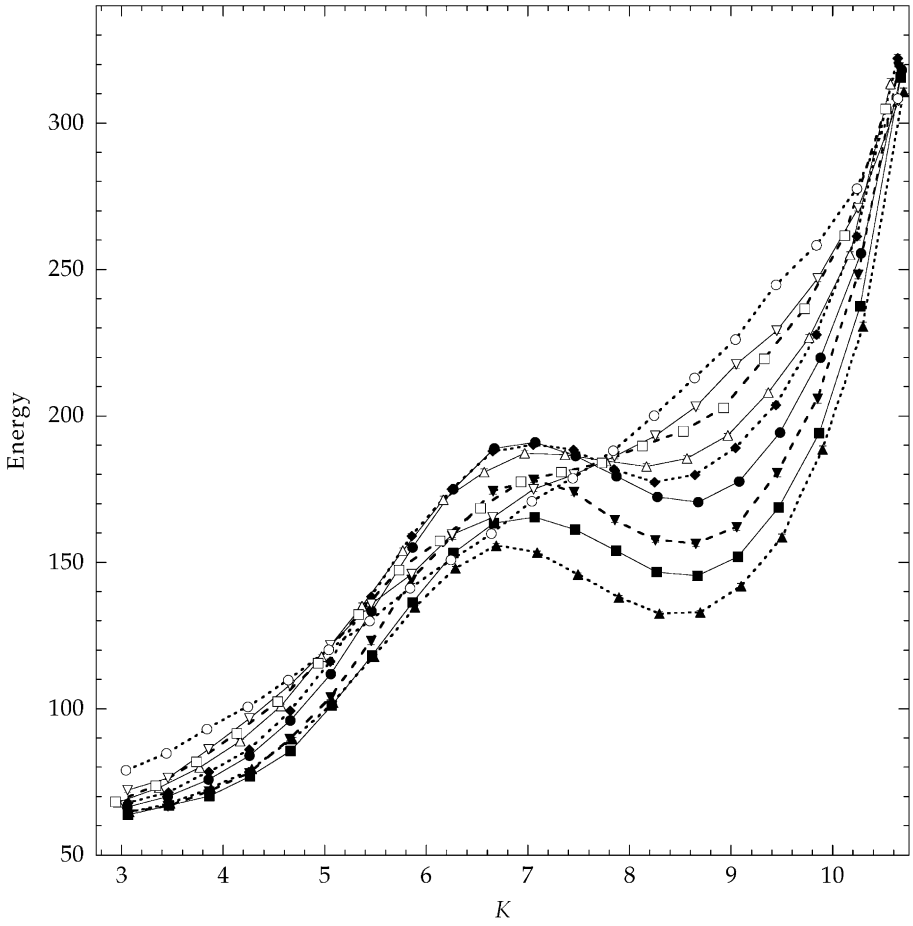

Fig. 3. Timing noise effects on $E(K)$ curves in the experiment. The dimensionless energy $E = \langle (p/2\hbar k_L)^2 \rangle / 2$ is plotted as a function of the stochasticity parameter K for several levels of timing noise. The noise levels are 0% (filled triangles, up), 0.5% (filled squares), 1% (filled triangles, down), 2% (filled circles), 3% (filled diamonds), 5% (open triangles, up), 8% (open squares), 10% (open triangles, down), and 20% (open circles), shown monotonically increasing in energy near $K = 8$. For this data set, the energy was measured after a sequence of 35 kicks.

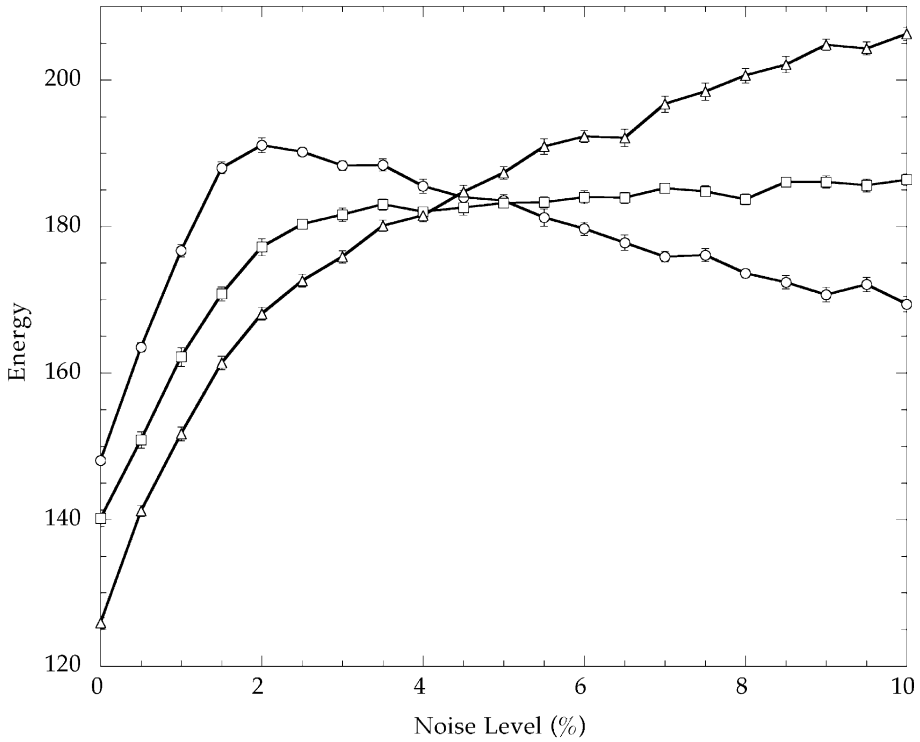

Fig. 4. Energy growth as a function of timing noise level in the experiment. The energy $E = \langle (p/2\hbar k_L)^2 \rangle /2$ is plotted as a function of the timing noise level for three levels of the stochasticity parameter K. The values of K are 6.8 (circles), 7.85 (squares), and 8.65 (triangles). For this data set, the energy was measured after a sequence of 35 kicks.

growth first rises and then falls as a function of the noise level, indicating that the noise becomes strong enough to break the correlations that give rise to that maximum. Indeed, one of the major effects of the noise is to wash out the oscillations in the curve, just as we saw in the amplitude noise case. It is clear from this data set that the rate of energy growth seen in Fig. 2 as a function of the noise level is not a universal feature, but depends upon the initial parameters chosen. Even in the absence of noise, it is most possible to observe clear dynamical localization in the first local minimum of the $E(K)$ curve, near $K = 8$. Outside of this region, the quantum dynamics can be influenced strongly by regions of anomalous diffusion in the corresponding classical dynamics.

Finally, in Fig. 4 we plot (for several values of K) curves that directly show the energy growth as a function of the noise level. The energy of the system is generally increased by the addition of low levels of noise, which destroy the fragile coherences that lead to dynamical localization. Higher levels of timing noise can either increase or decrease the energy of the system as the classical correlations are washed out. Naturally, the sign of this change depends upon whether we began at the peak or the valley of the undriven diffusion curve.

In conclusion, we have observed the effects of timing noise on the kicked-rotor system. A transition from quantum to qualitatively classical behavior appears as a universal growth in the system energy as low levels of noise are applied. For higher levels of noise, the system responds as a classical system might to the destruction of classical correlations, respectively increasing or decreasing the diffusion rate as the noise level is increased so as to approach random-phase limit behavior. It is hoped that this work will provide a basis for comparison with theory and will stimulate theoretical research in this field.

Acknowledgements

This work was supported by the NSF, the R. A. Welch Foundation, the US Israel Binational Science Foundation, the Sid W. Richardson Foundation, and the Fannie and John Hertz Foundation (D.A.S.).

References

[1] Zurek WH. Phys Today 1991;(October):36.
[2] Chapman MS, Hammond TD, Lenef A, Schmiedmayer J, Rubenstein RA, Smith E, Pritchard DE. Phys Rev Lett 1995;75:3783.
[3] Kokorowski DA, Cronin AD, Roberts TD, Pritchard DE. Phys Rev Lett 2001;86:2191.
[4] Brune M, Hagley E, Dreyer J, Maître X, Maali A, Wunderlich C, Raimond JM, Haroche S. Phys Rev Lett 1996;77:4887.
[5] Monroe C, Meekhof DM, King BE, Wineland DJ. Science 1996;272:1131.
[6] Blümel R, Reinhardt WP. Chaos in atomic physics. Cambridge; 1997.
[7] Ott E, Antonsen Jr. TM, Hanson JD. Phys Rev Lett 1984;53:2187.
[8] Dittrich T, Graham R. Europhys Lett 1987;4:263.
[9] Cohen D. Phys Rev A 1991;44:2249.
[10] Fishman S, Shepelyansky DL. Europhys Lett 1991;16:643.
[11] Shiokawa K, Hu BL. Phys Rev E 1995;52:2497.
[12] Arndt M, Buchleitner A, Mantegna RN, Walther H. Phys Rev Lett 1991;67:2435.
[13] Bayfield JE. Chaos 1991;1:110.
[14] Sirko L, Bellermann MRW, Haffmans A, Koch PM, Richards D. Phys Rev Lett 1993;71:2895.
[15] Koch PM. Physica D 1995;83:178.
[16] Clarke RM, Chan IH, Marcus CM, Duruöz CI, Harris Jr. JS, Campman K, Gossard AC. Phys Rev B 1995;52:2656.
[17] Graham R, Schlautmann M, Zoller P. Phys Rev A 1992;45:R19.
[18] Raizen M, Salomon C, Niu Q. Phys Today 1997;(July):30.
[19] Moore FL, Robinson JC, Bharucha C, Williams PE, Raizen MG. Phys Rev Lett 1994;73:2974.
[20] Moore FL, Robinson JC, Bharucha CF, Sundaram B, Raizen MG. Phys Rev Lett 1995;75:4598.
[21] Steck DA, Oskay WH, Raizen MG. Science 2001;293:274.
[22] Casati G, Chirikov BV, Ford J, Izrailev FM. Stochastic behaviour in classical and quantum hamiltonian systems. In: Casati G, Ford J, editors. Lecture notes in physics, vol. 93. Berlin: Springer; 1979.
[23] Klappauf BG, Oskay WH, Steck DA, Raizen MG. Phys Rev Lett 1998;81:1203;
Phys Rev Lett 1998;82:241(E).
[24] Milner V, Steck DA, Oskay WH, Raizen MG. Phys Rev E 2000;61:7223.
[25] Steck DA, Milner V, Oskay WH, Raizen MG. Phys Rev E 2000;62:3461.
[26] Ammann H, Gray R, Shvarchuck I, Christensen N. Phys Rev Lett 1998;80:4111.
[27] Fischer B, Rosen A, Bekker A, Fishman S. Phys Rev E 2000;61:R4694.
[28] Steck DA, Oskay WH, Raizen MG. Phys Rev Lett 2002;88:120406.
[29] Chirikov BV. Phys Rep 1979;52:263.
[30] Klappauf BG, Oskay WH, Steck DA, Raizen MG. Physica D 1999;131:78.
[31] Rechester AB, White RB. Phys Rev Lett 1980;44:1586;
Rechester AB, Rosenbluth MN, White RB. Phys Rev A 1981;23:2664.
[32] Klappauf BG, Oskay WH, Steck DA, Raizen MG. Phys Rev Lett 1998;81:4044.
[33] Chu S. Science 1991;253:861.
[34] DePue MT, McCormick C, Winoto SL, Oliver S, Weiss DS. Phys Rev Lett 1999;82:2262.
[35] Shepelyansky DL. Physica D 1987;28:103.